

AD-A143 131

TEMPERATURE DEPENDENCE OF THE RAMAN OH-STRETCHING
OVERTONE FROM LIQUID WATER(U) HOWARD UNIV WASHINGTON DC
LASER CHEMISTRY DIV W B MONOSMITH ET AL. 27 JUN 84
TR-19-ONR N00014-80-C-0305 F/G 7/4

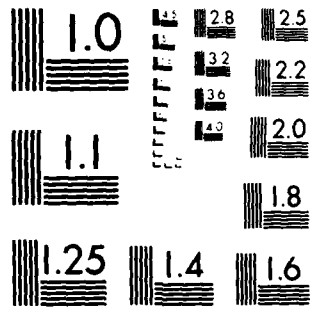
1/1

NL

UNCLASSIFIED



END
DATE
FILMED
8-84
DTIC



MICROCOPY RESOLUTION TEST CHART
NATIONAL BUREAU OF STANDARDS 1963-A

AD-A143 131

DTIC FILE COPY

SECURITY CLASSIFICATION OF THIS PAGE (When Data Entered)

REPORT DOCUMENTATION PAGE		READ INSTRUCTIONS BEFORE COMPLETING FORM
1. REPORT NUMBER <u>ONR-TR-192</u>	2. GOVT ACCESSION NO. <u>AD-A143 131</u>	3. RECIPIENT'S CATALOG NUMBER <u>6</u>
4. TITLE (and Subtitle) TEMPERAURE DEPENDENCE OF THE RAMAN OH-STRETCHING OVERTONE FROM LIQUID WATER		5. TYPE OF REPORT & PERIOD COVERED Technical Report 19
7. AUTHOR(s) W.B. Monosmith and G.E. Walrafen		6. PERFORMING ORG. REPORT NUMBER
9. PERFORMING ORGANIZATION NAME AND ADDRESS Laser Chemistry Division Department of Chemistry Howard University/ Washington, D.C. 20059		8. CONTRACT OR GRANT NUMBER(s) N00014-80-C-0305
11. CONTROLLING OFFICE NAME AND ADDRESS Office of Naval Research Department of the Navy Arlington, VA 22217		10. PROGRAM ELEMENT, PROJECT, TASK AREA & WORK UNIT NUMBERS NR-051-733
14. MONITORING AGENCY NAME & ADDRESS (if different from Controlling Office)		12. REPORT DATE June 27, 1984
		13. NUMBER OF PAGES 8
		15. SECURITY CLASS. (of this report) Unclassified
		16. DECLASSIFICATION/DOWNGRADING SCHEDULE
16. DISTRIBUTION STATEMENT of this Report: Approved for public release; reproduction is permitted for any purpose of the United States Government; distribution is unlimited.		
17. DISTRIBUTION STATEMENT (of the abstract entered in Block 20, if different from Report) Distribution of this document is unlimited.		
18. SUPPLEMENTARY NOTES Prepared for publication in the Journal of Physical Chemistry.		
19. KEY WORDS (Continue on reverse side if necessary and identify by block number) Water Structure, OH Overtone, Raman Spectroscopy		
20. ABSTRACT (Continue on reverse side if necessary and identify by block number) The first Raman overtone of the OH-stretching vibration from highly purified liquid water has been examined quantitatively in the temperature range of 20-95°C, and at frequencies from about 5500-8000 cm ⁻¹ . <u>5500-8000/cm⁻¹</u>		

JUL 17 1984
A

DD FORM 1473 1 JAN 73 EDITION OF 1 NOV 65 IS OBSOLETE S/N 0102-014-6601

84 07 16 075

SECURITY CLASSIFICATION OF THIS PAGE (When Data Entered)

Temperature dependence of the Raman OH-stretching overtone from liquid water

W. B. Monosmith and G. E. Walrafen

Department of Chemistry, Howard University, Washington D. C. 20059

The first Raman overtone of the OH-stretching vibration from highly purified liquid water has been examined quantitatively in the temperature range of 20–95 °C, and at frequencies from about 5500–8000 cm^{-1} . The overtone Raman spectra show contour shapes, depolarization ratio dispersion, and an isosbestic frequency ($6960 \pm 25 \text{ cm}^{-1}$, uncorrected; $6900 \pm 25 \text{ cm}^{-1}$, density and refractive index corrected) which, apart from the effects of anharmonicity, tend to mimic the fundamental, including its major four-component substructure. The two components at about 7030 and 6850 cm^{-1} were interpreted, respectively, in terms of nonhydrogen-bonded OH, and triply hydrogen-bonded OH groups, which are common to the three-bonded H_2O species, whereas two components at about 6665 and 6160 cm^{-1} were interpreted as intermolecular coupling components of the fully hydrogen-bonded, i.e., four-bonded H_2O species. A ΔH° value of -2.5 Kcal/mol hydrogen bond was obtained from the temperature dependence of ratios of the combined component intensities of these two pairs, in agreement with results from previous Raman fundamental measurements. The feature near 6160 cm^{-1} was found to be better resolved in the spectrum than its fundamental analog, indicating that anharmonicity is advantageous in elucidating contour substructure.

I. INTRODUCTION

The overtones of the OH-stretching vibration from liquid water have been studied for many years by infrared techniques, and some of the most thorough infrared overtone work on aqueous systems has been reported by Luck and co-workers.¹ The infrared spectra of liquid H_2O , D_2O , and HDO are characterized by a large number of intense overtone and combination bands.^{1,2} Unfortunately, the Raman OH-overtone spectrum is extremely weak, and thus all of the Raman work was restricted, until recently,^{3,4} to the fundamental region of the spectrum (i.e., below $\sim 4000 \text{ cm}^{-1}$).

The OH-stretching vibration has been found to be very sensitive to the details of the hydrogen bonding in water.³⁻⁸ This sensitivity is useful because it gives rise to spectral features related to various perturbations of the OH vibration. Unfortunately a unique interpretation of the observed broad spectral features has been difficult to achieve. The available data for the most part are supportive of a mixture model involving hydrogen-bonded species, plus OH groups that are essentially free, but some workers have not entirely abandoned continuum models.⁹ However, because the free OH groups and the hydrogen-bonded species, particularly the latter, are distributed in frequency, it is evident that the mixture and continuum descriptions are, in some regards at least, a matter of semantics.

Two further mechanisms, namely, Fermi resonance and intermolecular coupling have led to contour breadth and have caused problems in interpretation. Fermi resonance may occur because the symmetric stretching vibration of the H_2O molecule has the same A_1 symmetry species as the overtone of the bending vibration. Intermolecular coupling arises from the coupling that nearby oscillators experience when they are strongly perturbed by hydrogen bonds. The

Fermi resonance effects have never been unequivocally isolated in the spectrum, although clear evidence for intermolecular coupling has recently been developed from dilution experiments.^{10,11}

The Raman OH-stretching overtone spectrum has recently been reported for liquid water by Beisley and Sceats.³ Their results, however, were complicated by the presence of an intense sloping background due to fluorescence from an impurity. We now present new results based on Raman data which represent a considerable improvement over those previously reported.³ This improvement resulted from the use of very rigorously purified water, which lowered the fluorescence level, and also from relatively higher³ Raman signal levels, resulting from high (4.5 W, 488 nm) laser power levels.

Our improved Raman OH-stretching overtone results show new features (e.g., a broad, strongly polarized component is now seen toward the low-frequency side of the OH peak). This new feature is thought to be the analog of the shoulder observed in the fundamental spectrum near $\sim 3250 \text{ cm}^{-1}$. Our spectra also show an isosbestic frequency in the temperature range 20–95 °C which agrees with reported infrared overtone isosbestic values,¹ and which is consistent with isosbestic frequencies obtained from the fundamental Raman region of liquid water.^{11,12} We also have measured depolarization ratios over the entire frequency range of the OH-stretching overtone contour.

The details of the present results follow, but the significant feature of the improved Raman data is that they seem to demand the conventional picture of an overtone region which essentially shows the free OH and broad hydrogen-bonded species contributions, plus coupling effects, all as modified by various degrees of anharmonicity across the overtone contour. This picture contrasts strongly with the

recently proposed explanation which stemmed from data of lower reliability and smaller frequency range.³

II. EXPERIMENTAL PROCEDURES

Overtone Raman spectra were obtained from highly purified water kindly provided by M. Bennett of the Naval Research Laboratory, Washington, D. C. The water was filtered and deionized prior to triple distillation in a fused silica still. The sloping background reported earlier in the Raman spectrum,³ still persisted to some extent when this water was used, but it was greatly reduced. For ordinary distilled water, the intense fluorescence background level becomes even more pronounced as the temperature rises, and it may increase by 2 or 3 times its original intensity at 95 °C. Rigorous purification, however, lowers this effect as well. It is also important to clean the water storage container and the Raman cell with chromic acid solution prior to use.

Raman spectra were obtained with a *J-Y* double-monochromator and a cooled Hamamatsu R928 photomultiplier tube. A Spectra-Physics model 171 argon ion laser was used for excitation. It delivered approximately 4.5 W of vertically polarized 488 nm light at the sample. For polarization measurements, a sheet polarizer was inserted in front of the collection optics. A polarization scrambler was also employed in front of the entrance slit. A photon counting system was employed with a Nicolet model 1170 multichannel analyzer. Slit widths corresponding to 16 cm⁻¹ were used for all spectra.

Decompositions of spectra using Gaussian components was accomplished using a duPont 310 analog computer.

III. EXPERIMENTAL RESULTS

Raman OH-stretching overtone (first overtone) spectra representative of the *S*/*N* ratio and fluorescence background level generally obtained in this work are shown in Fig. 1 for pure liquid water at 20 °C. The spectra are very weak, despite the fact that they were obtained with a slit width corresponding to 16 cm⁻¹ and a power level of 4.5 W at the sample. The number of counts per second recorded at the intensity maximum (without using the polarization analyzer) was about 1000 counts/s, of which approximately 750 counts/s resulted from Raman processes, with approximately 250 counts/s

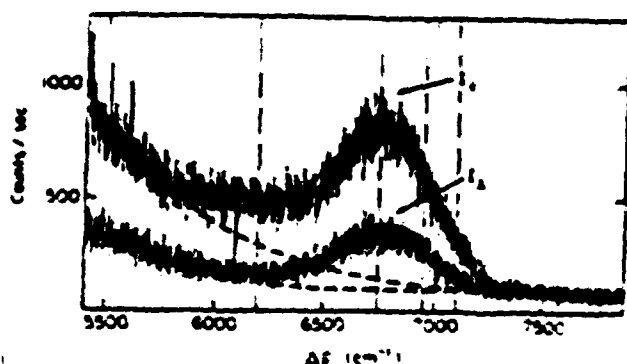


FIG. 1. Raman OH-stretching overtone spectra from liquid water at 20 °C (Raw data). $I_{||}$ refers to the polarized spectrum, and I_{\perp} to the depolarized spectrum. Dashed vertical lines refer to peaks, shoulders, or inflections.

resulting primarily from fluorescence due to impurities. The intensity of the OH-stretching overtone was observed to be about 10⁻⁶ times that of the corresponding fundamental, see also Ref. 12. This weakness, of course, is partly instrumental, because the overtone contour ranges from 670–770 nm (with 488 nm excitation) where the photomultiplier response, grating efficiency, and geometrical optical spectrometer conditions (e.g., curved slit image scanned by a straight slit) are all unfavorable. Nevertheless, the present signal-to-background ratio of approximately 3 represents a significant improvement over the estimated ratio of 0.8 obtained by Belsley and Seaton.³ Furthermore, our background-corrected (Raman) signal is about four times larger than theirs. We recognize, nevertheless, that the weakness of our spectra still limits the amount of quantitative information that can be extracted, compared to the fundamental. Hence, only those features that were found to be common in numerous repetitions of the spectra are considered reliable. Any mention of features relative to a specific spectrum will imply this general reproducibility.

The polarized spectrum of Fig. 1 $I_{||}$ shows an intensity maximum near 6750 cm⁻¹, with an inflection near 7100 cm⁻¹ suggestive of a high-frequency shoulder, and a very broad tail centered near 6200 cm⁻¹ indicative of a low-frequency component. The depolarized spectrum I_{\perp} , shown below in Fig. 1, peaks near 6750 cm⁻¹ and shows a low-frequency tail like the $I_{||}$ spectrum, but it also gives evidence of a high-frequency inflection or shoulder near 6950 cm⁻¹. Thus, reproducible physical evidence exists that would indicate that the OH-overtone contour is composed of at least four broad components at ~6200, ~6750, ~6950, and ~7100 cm⁻¹ at 20 °C. Various aspects of the spectra relating to four components near these frequencies are developed subsequently in this work.

Nonlinear baselines under the $I_{||}$ and I_{\perp} spectra are shown by dashed lines in Fig. 1. These baseline estimates were obtained by examinations of a wide frequency range. Their curvature is gradual compared to any Raman features ascertained from their use. We regard intensities above these baselines to represent the true Raman intensity, within our present ability to obtain it. The intensity profiles were smoothed and baseline subtraction was accomplished. Correction for effects of temperature on refractive index and density was then made.¹¹ No attempt to obtain isotropic spectra (i.e., $I_{||} = (4I_{\perp}/3)$) was made here, because of uncertainties in the $I_{||}$ and I_{\perp} spectra.

Depolarization ratios $\rho = I_{\perp}/I_{||}$ are plotted vs Raman frequency shift in cm⁻¹ $\Delta\delta$ in Fig. 2 (20 °C). Baseline uncertainties are less important here because they tend to cancel, provided that they are consistent in shape for $I_{||}$ and I_{\perp} . However, the decreasing *S*/*N* ratio in the wings of the contour leads to correspondingly large errors (shown by bars). Despite such errors, the Fig. 2 data represent the first OH-overtone depolarization measurement made below 6400 cm⁻¹ for liquid water.

The maximum depolarization ratio occurs near 6740 ± 50 cm⁻¹. Also the existence of a highly polarized component near 6200 cm⁻¹ is obvious, compare also with Fig. 1. A highly polarized low-frequency component near

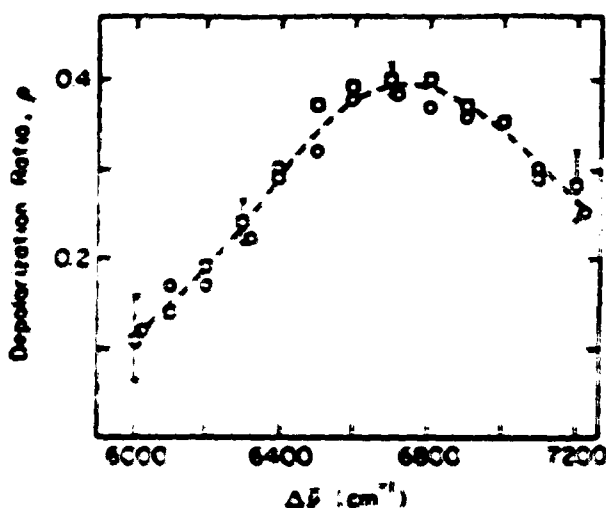


FIG. 2. Depolarization ratio ρ as a function of Raman frequency at 20 °C. Duplicate determinations, \circ and \ominus .

3250 cm^{-1} also occurs as a shoulder on the OH-stretching fundamental. This feature is probably the analog of the 6200 cm^{-1} shoulder.

In contrast to the data of Fig. 2, Belsley and Seasty concluded from measurements between 6000 and 7200 cm^{-1} that the depolarization ratio was nearly constant and equal to ~ 0.4 . Their conclusion and interpretation arising from it must now be regarded as untenable in view of the present data.

In Fig. 3 four overtone Raman spectra are shown which correspond to temperatures between 20 and 95 °C. The integrated Raman intensities of this figure are quantitatively comparable to $\sim 2\%$.

The Fig. 3 results comprise one of two series of runs accomplished at four temperatures between 20 and 95 °C. A third series of runs was also carried out at six temperatures. Within an intensity accuracy of $\sim 2\%$, no differences were observed between corresponding spectra from these three series.

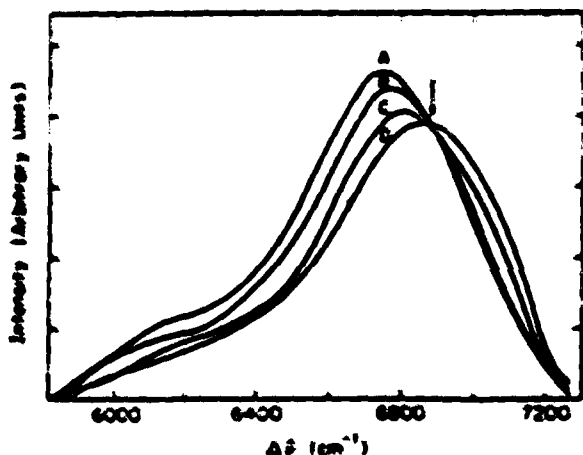


FIG. 3. Four overtone Raman spectra at different temperatures showing an anharmonic frequency indicated by the arrow. The letters correspond to the following temperatures: (A) 20 °C, (B) 45 °C, (C) 70 °C, (D) 95 °C.

Tests for long-term intensity drift were also made. One of the series involving four temperatures (Fig. 3) was begun at 95 °C. Successive runs were conducted at decreasing temperatures to 20 °C. Then the measurements were repeated in reverse temperature sequence, from 20 to 95 °C. Spectra corresponding to the same temperature were found to be comparable to within 1% at the intensity maximum, and to 2% or better in the integrated intensity, despite the fact that the time interval between the 95 °C pair was about 10 h.

Baselines for the Fig. 3 spectra were determined as described previously. Smooth curves were drawn through the spectra by averaging the noise excursions. The smooth curves were then digitized using a HP-47 computer. The digital data were corrected for variations in density and refractive index, $\frac{dn}{dc}$ replotted using a HP-7470 plotter (Fig. 3).

In addition to evidence cited previously for four contour components, the corrected spectra of Fig. 3 provide evidence for a fifth physical observable, namely, a region of crossing, or an anisotropic frequency, near 6900 $\pm 25 \text{ cm}^{-1}$. However, an isotropic frequency was also found for the uncorrected spectra near 6940 $\pm 25 \text{ cm}^{-1}$. In regard to this, Lack¹ has reported an infrared isotropic frequency for pure H_2O which occurs (without correction) at 6945 cm^{-1} . The uncorrected infrared and Raman values of 6945 cm^{-1} and 6940 $\pm 25 \text{ cm}^{-1}$, respectively, thus compare favorably. Also the fact that the infrared and Raman overtone spectra show common isotropic frequencies indicates that both spectra measure the equilibrium¹⁰ between different hydrogen-bonded species (e.g., four-bonded to three-bonded) as previously concluded from studies of the infrared and Raman fundamentals.

Gaussian decompositions of the Raman OH-stretching fundamental from pure water have been reported previously using four major components.^{14,15} Similar four-Gaussian decompositions were accomplished in this work for the overtone spectra at temperatures from 20 to 95 °C. To achieve these decompositions, however, it was important to apply specific criteria which resulted from past experience with the OH fundamental. These six criteria are detailed here in Ref. 16.

A typical four-Gaussian decomposition of the OH-overtone spectrum corresponding to 65 °C is shown in Fig. 4. This decomposition and other similar decompositions of spectra obtained from 20 to 95 °C, were found to meet the criteria listed in Ref. 16. However, as a further test of the component frequencies, it is useful to examine Table I.

In Table I Raman frequency values corresponding to Gaussian component centers are compared for fundamental and overtone OH regions of pure H_2O . A measure of the % anharmonicity is included, namely, $100(2B-A)/2B$, where $2B$ is the first harmonic frequency, i.e., twice the fundamental frequency B and A is the frequency of the first overtone.

In regard to Table I and also to Fig. 4 it should be noted that the Gaussian components are designated from (1) to (4) in order of increasing frequency. This ordering scheme applies to the OH overtone components as well as to the OH fundamental components, and it is employed extensively below.

As seen from Table I, three overtone components at 7030, 6850, and 6665 cm^{-1} have anharmonicities of $\sim 3\%$.

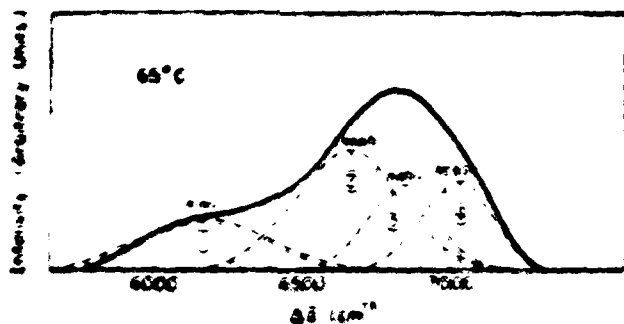


FIG. 4. Raman spectrum at 65°C showing the decomposition into four Gaussian components 1-4 defined in the text.

which distinguishes them from the component at 6160 cm^{-1} whose anharmonicity is higher $\sim 5\%$. This division of components according to anharmonicity provides support for the subsequent assignment of the 6160 cm^{-1} component.

Integrated Gaussian component intensities are plotted vs temperature in $^{\circ}\text{C}$ in Fig. 5. The intensities of components (1) and (2) I_1 and I_2 decrease with temperature rise, whereas the opposite dependence is observed for the component (4) intensity I_4 . The intensity of component (3) I_3 is roughly constant from 20 to 95 $^{\circ}\text{C}$. This near constancy is discussed subsequently.

In Fig. 6 $\ln(I_2/I_1)$, where $I_2 = I_4 = I_3$ and $I_1 = I_2 = I_3$, is plotted vs $1/T$. The straight line shown represents the linear least-square fit of the data, and its slope corresponds to a ΔH° value of $\Delta H^{\circ} = 2.5 \text{ kcal/mol}$ in excellent agreement with other reported values which correspond to a mole of hydrogen bonds.¹⁰ Other plots were also constructed using individual component intensities, but the method used for Fig. 6 may be the most reliable because the sums $I_2 = I_4$ and $I_1 = I_3$ are subject to smaller errors than the individual component intensities.

IV. DISCUSSION

A. General Assignment

In this work four reproducible contour features were observed visually from the combined polarized and depolarized Raman OH-overtone spectra near ~ 6300 , ~ 6750 , ~ 6950 , and $\sim 7100 \text{ cm}^{-1}$, see Fig. 1 and its discussion.

TABLE I. Comparison of overtone and fundamental Gaussian component frequencies, % anharmonicity shown in last column to the right. Frequencies corresponding to maximum depolarization ratio ρ_{max} and minimum frequency ν_{min} are compared below. Components are designated by numbers in parentheses, first column to the left.

	A	B	$100\Delta\nu/\nu_{\text{min}}$
(4)	7050	3625 (7225)	3%
(3)	6950	3510 (7000)	3%
(2)	6665	3425 (6870)	3%
(1)	6160	3120 (6260)	3%
	$\rho_{\text{max}} @ 6740$ $\nu_{\text{min}} = 6700$	$\rho_{\text{max}} @ 3550$ $\nu_{\text{min}} = 3480$	

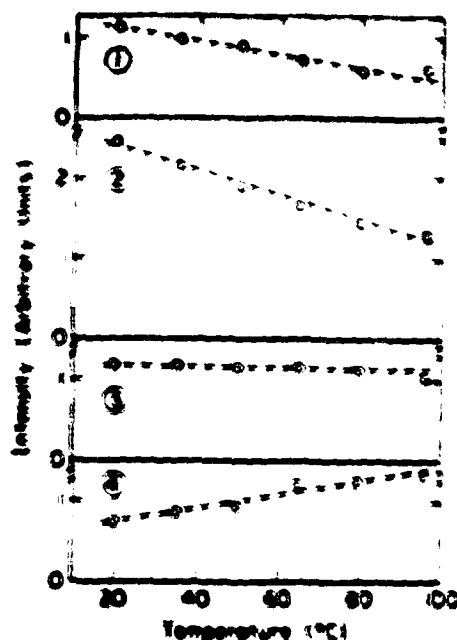


FIG. 5. Integrated Gaussian component intensities as a function of temperature. For component frequencies 1-4 see Fig. 4 or Table I.

However, when the overlaid contours were decomposed using four Gaussian components, the corresponding component centers actually occurred near 6160, 6665, and 7050 cm^{-1} , and these values are regarded as more accurate than the visually observed features. From Table I it is probable that these four Gaussian components are the analogs of the four Gaussian components from the fundamental at 3250, 3425, 3550, and 3625 cm^{-1} , respectively.¹⁰ Thus, in agreement with a previous fundamental assignment,¹⁰ component (1) at 6160 cm^{-1} is assigned to intermolecular coupling, component (2) at 6665 cm^{-1} to fully hydrogen-bonded four-bonded H_2O molecules, component (3) at 6950 cm^{-1} to three-bonded (one hydrogen bond disrupted) H_2O mole-

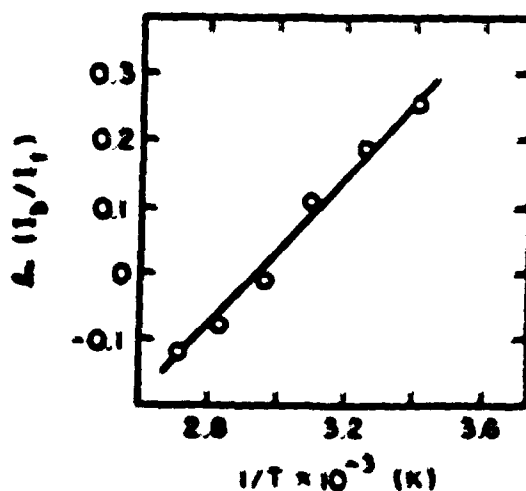


FIG. 6. Ratio of $\ln(I_2/I_1)$ vs $1/T$ for definitions of I_2 and I_1 . The straight line represents the linear least-square fit of the data, and corresponds to a ΔH° value of $\Delta H^{\circ} = 2.5 \text{ kcal/mol}$.

cules, and component (4) at 7030 cm^{-1} to nonhydrogen-bonded OH oscillators (i.e., to the nonhydrogen-bonded OH of the three-banded entity). (More detailed assignments for components (1) and (2) at 6160 and 6665 cm^{-1} are given subsequently.) Component (3), however, may also contain hydrogen-bonded contributions from four- and six-banded H_2O molecules (i.e., the nonhydrogen-bonded OH groups of the four- and six-banded molecules) and contribute to component (4).

The production of three-banded H_2O molecules from four-banded H_2O molecules is shown schematically in Fig. 7, where the four-banded H_2O molecule on the left is indicated by a closed dashed curve. The three-banded H_2O molecule on the right is indicated by the open dashed curve, and the nonhydrogen-bonded or dangling OH is emphasized by a heavy line. The H_2O molecules shown, for example, on the left, outside of the dashed curve, are fully hydrogen-bonded but the hydrogen bonds are omitted for simplicity.

B. Assignments of components (3) and (4)

As shown in Fig. 7 the production of three-banded H_2O from four-banded H_2O involves the formation of a species with one nonhydrogen-bonded or dangling OH group. The other OH group of this three-banded species of C_{2v} symmetry is involved in three hydrogen bonds. The dangling OH group of this C_{2v} species is thought to produce component (3), i.e., the 3635 cm^{-1} fundamental component, and the corresponding 7030 cm^{-1} overtone component. The triple hydrogen-bonded OH group of this species is thought to produce component (4), i.e., the 3450 cm^{-1} component in the fundamental and the corresponding 6900 cm^{-1} component in the overtone. It should be mentioned here, however, that the hydrogen bond involving the proton of the three-banded OH group is probably much more effective in perturbing the OH stretching frequency than interactions at the lone pair oxygen electron, because the hydrogen bond may be nearly co-linear with the OH bond. This effect is discussed below in relation to the NDO molecule.

C. Assignments of components (1) and (2)

The central H_2O molecule of the four-banded entity shown to the left in Fig. 7 would, if free, give rise to a symmetric stretching motion (A, species of the C_{2v} point group) and to an asymmetric stretching motion (B, species). The asymmetric stretching motion, however, seems never to have been unequivocally identified for liquid water. It would

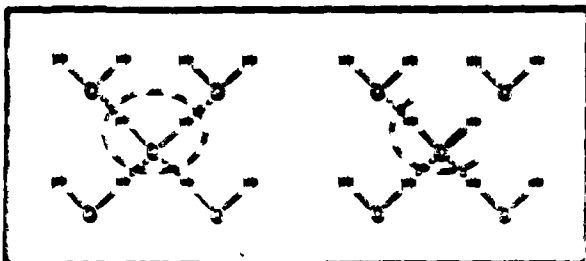


FIG. 7. Schematic diagram representing formation of three-banded H_2O molecules from four-banded H_2O molecules.

be weak in the Raman spectrum, and it may be unresolved from component (3), namely, the fundamental and overtone components at 3530 and 6650 cm^{-1} due to the triple hydrogen-bonded OH group. Also, if A, B, from four-banded H_2O is unresolved from component (3) of three-banded H_2O , it is apparent that the weakness constantly discussed relative to Fig. 5 is explained.

If the asymmetric stretching motion for liquid water occurs near component (3), an explanation for the remaining two components (1) and (2) is required. A possible assignment for component (1) involves Fermi resonance, but this assignment is not greatly favored for reasons described subsequently. An assignment for components (1) and (2) that is considered to be in agreement with observed depolarization ratios,¹² with dilution studies involving NDO,¹³ and with effects of electrolyte addition¹⁴ follows.

Component (1) is assigned to a tetrahedral grouping of five hydrogen-bonded H_2O molecules whose symmetric stretches are all in-phase (Fig. 7, left). Component (2) is also assigned to symmetric stretching, but in this case some of the symmetric stretches of the five H_2O molecules are out-of-phase. The H_2O molecules giving rise to component (2) are thus decoupled to some extent, hence component (2) would be expected to persist under conditions of dilution or of structure-breaking electrolyte addition when component (1) is very weak or absent. For example, the breakdown of hydrogen bonds in the strong intermolecular decoupling in the case of NDO would tend to be expected to reduce the intensity of component (1) while only slightly affecting component (2).

Examination of Fig. 7 left structure in relation to the assignment of component (1) indicates that the combined in-phase symmetric stretches of the five H_2O molecules shown would be the overall symmetry of the five-molecule unit is C_{2v} , i.e., T_2 in the oxygen atom, corresponds to a totally symmetric stretching motion of A₁ symmetry. The depolarization ratio for this mode might be expected to tend toward zero—the observed value is 0.04 .¹² On the other hand, the out-of-phase symmetric stretches would lead to B₂ symmetry and the corresponding depolarization ratio might tend toward 0.75 , except for the decoupling mentioned. This decoupling among the H_2O molecules involved to yield a depolarization ratio well below 0.75 , as expected for the symmetric stretches of individual H_2O molecules. The experimental depolarization value for the fundamental component (1) is 0.3 .¹²

In relation to intermolecular decoupling, the right structure of Fig. 7 should also be mentioned. If the lone proton of the central H_2O molecule (i.e., the hydrogen-bonded proton) were replaced by deuterium, the hydrogen-bonding along the OD bond which is a major effect compared to that involving the lone pair electrons of the central atom would not be coupled with the motion of the dangling or nonhydrogen-bonded proton. Hence this OD stretch would be expected to assume a "normal" hydrogen-bonded or four-banded value near 2525 cm^{-1} . This means that the analogous OH value would be near the four-banded value of 3450 cm^{-1} , not at 3530 cm^{-1} . Thus, in dilute NDO, not only is the totally in-phase component (1) weak, but component (3) is weak

as well as observed previously in comparisons involving HDO, D₂O, and H₂O.¹⁷

B. Other Assignments

Component (1) has often been assigned to Fermi resonance, i.e., the overtone of 2_v1 engages in resonance with ν₂, because both are of 1 species. However, in the case of OH species the assignment would require that 2_v1 engage in Fermi resonance with 2_v1. Such resonance would require that 2_v1 be of the same symmetry as the overtone component 1, relative to the other overtone components. The overtone 2_v1, however, has optical phonon modes, and such a low-phonon mode should be extremely weak, compared to the two-phonon modes that make up the OH overtone spectrum.

V. SUMMARY

The complete OH overtone laser spectrum region from 5500-6000 cm⁻¹ has been examined from 20 to 45 °C. Contour subtraction is indicated with temperatures indicated near (1) 6140 cm⁻¹, (2) 5985 cm⁻¹, (3) 5850 cm⁻¹, and (4) 5710 cm⁻¹. An anomalous frequency corrected for density and refractive index was observed at 6100 ± 25 cm⁻¹. This anomalous frequency is indicative of an equilibrium between different hydrogen bonded species, believed to be mostly four-bonded and three-bonded, in the temperature range studied. Plots of the four component frequencies vs temperature are also indicative of a four-bonded to three-bonded equilibrium, and a logarithmic plot comparing component 1k (where k = 1, 2, 3, 4) to component 1k (where k = 1, 2, 3, 4) yields a 2.87 slope if k = 2. This plot of hydrogen bonds in agreement with other reported values. All of the observations of this work are thus indicative of an equilibrium between species, contrary to the previous interpretations of Britney and Swann, but in agreement with Luck and others.

ACKNOWLEDGMENT

This work was supported by contracts from the Office of Naval Research.

¹⁶ W. P. Luck and W. D. Swann, *J. Chem. Phys.* **20**, 1043 (1952).
¹⁷ D. Schwab, C. Bernheim, and W. P. Luck, *Spectroscopy*, **18**, 12 (1973).

¹⁸ W. D. Swann and W. P. Luck, *J. Chem. Phys.* **19**, 1043 (1951).

¹⁹ W. D. Swann and W. P. Luck, *J. Chem. Phys.* **20**, 1043 (1952).

²⁰ W. D. Swann, *J. Chem. Phys.* **21**, 1043 (1953).

²¹ W. D. Swann, *J. Chem. Phys.* **22**, 1043 (1954).

²² W. D. Swann, *J. Chem. Phys.* **23**, 1043 (1955).

²³ W. D. Swann, *J. Chem. Phys.* **24**, 1043 (1956).

²⁴ J. R. Durig, *J. Chem. Phys.* **55**, 1043 (1971).
²⁵ J. R. Durig, *J. Chem. Phys.* **56**, 1043 (1972).
²⁶ J. R. Durig, *J. Chem. Phys.* **57**, 1043 (1973).
²⁷ J. R. Durig, *J. Chem. Phys.* **58**, 1043 (1974).

²⁸ J. R. Durig, *J. Chem. Phys.* **59**, 1043 (1975).

²⁹ J. R. Durig, *J. Chem. Phys.* **60**, 1043 (1976).

³⁰ J. R. Durig, *J. Chem. Phys.* **61**, 1043 (1977).

³¹ J. R. Durig, *J. Chem. Phys.* **62**, 1043 (1978).

³² J. R. Durig, *J. Chem. Phys.* **63**, 1043 (1979).

³³ J. R. Durig, *J. Chem. Phys.* **64**, 1043 (1980).

³⁴ J. R. Durig, *J. Chem. Phys.* **65**, 1043 (1981).

³⁵ J. R. Durig, *J. Chem. Phys.* **66**, 1043 (1982).

³⁶ J. R. Durig, *J. Chem. Phys.* **67**, 1043 (1983).

³⁷ J. R. Durig, *J. Chem. Phys.* **68**, 1043 (1984).

³⁸ J. R. Durig, *J. Chem. Phys.* **69**, 1043 (1985).

³⁹ J. R. Durig, *J. Chem. Phys.* **70**, 1043 (1986).

⁴⁰ J. R. Durig, *J. Chem. Phys.* **71**, 1043 (1987).

⁴¹ J. R. Durig, *J. Chem. Phys.* **72**, 1043 (1988).

⁴² J. R. Durig, *J. Chem. Phys.* **73**, 1043 (1989).

⁴³ J. R. Durig, *J. Chem. Phys.* **74**, 1043 (1990).

⁴⁴ J. R. Durig, *J. Chem. Phys.* **75**, 1043 (1991).

⁴⁵ J. R. Durig, *J. Chem. Phys.* **76**, 1043 (1992).

⁴⁶ J. R. Durig, *J. Chem. Phys.* **77**, 1043 (1993).

⁴⁷ J. R. Durig, *J. Chem. Phys.* **78**, 1043 (1994).

⁴⁸ J. R. Durig, *J. Chem. Phys.* **79**, 1043 (1995).

⁴⁹ J. R. Durig, *J. Chem. Phys.* **80**, 1043 (1996).

⁵⁰ J. R. Durig, *J. Chem. Phys.* **81**, 1043 (1997).

⁵¹ J. R. Durig, *J. Chem. Phys.* **82**, 1043 (1998).

⁵² J. R. Durig, *J. Chem. Phys.* **83**, 1043 (1999).

⁵³ J. R. Durig, *J. Chem. Phys.* **84**, 1043 (2000).

⁵⁴ J. R. Durig, *J. Chem. Phys.* **85**, 1043 (2001).

⁵⁵ J. R. Durig, *J. Chem. Phys.* **86**, 1043 (2002).

⁵⁶ J. R. Durig, *J. Chem. Phys.* **87**, 1043 (2003).

⁵⁷ J. R. Durig, *J. Chem. Phys.* **88**, 1043 (2004).

⁵⁸ J. R. Durig, *J. Chem. Phys.* **89**, 1043 (2005).

⁵⁹ J. R. Durig, *J. Chem. Phys.* **90**, 1043 (2006).

⁶⁰ J. R. Durig, *J. Chem. Phys.* **91**, 1043 (2007).

⁶¹ J. R. Durig, *J. Chem. Phys.* **92**, 1043 (2008).

⁶² J. R. Durig, *J. Chem. Phys.* **93**, 1043 (2009).

⁶³ J. R. Durig, *J. Chem. Phys.* **94**, 1043 (2010).

⁶⁴ J. R. Durig, *J. Chem. Phys.* **95**, 1043 (2011).

⁶⁵ J. R. Durig, *J. Chem. Phys.* **96**, 1043 (2012).

⁶⁶ J. R. Durig, *J. Chem. Phys.* **97**, 1043 (2013).

⁶⁷ J. R. Durig, *J. Chem. Phys.* **98**, 1043 (2014).

⁶⁸ J. R. Durig, *J. Chem. Phys.* **99**, 1043 (2015).

⁶⁹ J. R. Durig, *J. Chem. Phys.* **100**, 1043 (2016).

⁷⁰ J. R. Durig, *J. Chem. Phys.* **101**, 1043 (2017).

